

ELECTRONIC SUPPORTING INFORMATION

**A sustainable approach to energy storage in buildings:
the first rechargeable geopolymmer-based battery**

Vadim M. Kovrugin ^{*,ab§} Liliane Guerlou-Demourgues ^{ab} Laurence Croguennec ^{abc} Jorge S. Dolado ^{de}
and Cyril Aymonier ^{abc}

^a Univ. Bordeaux, CNRS, Bordeaux INP, ICMCB, UMR 5026, 33600 Pessac, France.

^b RS2E, Réseau Français sur le Stockage Electrochimique de l'Energie, FR CNRS 3459, 80039 Amiens Cedex 1, France.

^c ALISTORE-ERI European Research Institute, CNRS FR 3104, 80039 Amiens Cedex 1, France.

^d Centro de Física de Materiales (CSIC-UPV/EHU)-Material Physics Centre (MPC), Paseo Manuel de Lardizabal 5, 20018 San Sebastian, Spain.

^e Donostia International Physics Center (DIPC), 20018 San Sebastian, Spain.

[§] Present address: Université de Caen Normandie, ENSICAEN, CNRS UMR 6508, CRISMAT, Normandie Univ., 14000 Caen, France.

Table of contents

Table S1. Chemical composition of the metakaolin geopolymers	S2
Figure S1. EIS spectra of various electrolytes at room temperature	S2
Table S2. Ionic conductivity of various electrolytes.....	S2
Figure S2. CV plots and corresponding second derivatives	S3
Figure S3. CV plots at 0.2 mV/s for four different cells.....	S3
Figure S4. Evolution of the CV plots at 0.2 mV/s corresponding to four different cell.....	S4
Figure S5. Experimental powder XRD pattern for EMD-MnO ₂ and simulated XRD patterns for selected MnO ₂ polymorphs:	S4
Figure S6. Simulated XRD patterns for selected Mn-containing phases reported in the Zn/MnO ₂ system: ZnMn ₂ O ₄ ⁵ (a), H _x Mn ₂ O ₄ ⁶ (b), γ-MnOOH ⁷ (c), α-MnOOH ⁷ (d), and ZnMn ₃ O ₇ (H ₂ O) ₃ ⁸ (e).	S5
Figure S7. Phase identification in experimental <i>ex situ</i> XRD patterns of the MnO ₂ electrode at different voltages upon electrochemical cycling	S6
Figure S8. Phase identification in experimental <i>ex situ</i> XRD patterns of the solid electrolyte at different voltages upon electrochemical cycling	S7
Figure S9. Photos of the cell after cycling	S8
Figure S10. Specific capacity <i>versus</i> cycle number in three voltage ranges.....	S8

Figure S11. Charge/discharge curves with different curing time and under various cycling conditions.....	S9
Figure S12. Current rate capabilities at C-rates from 0.04 to 1C	S9
Figure S13. Mass loss of the metakaolin-based batteries over time.....	S10
Figure S14. Powering LEDs by two geopolymers cells connected in series.....	S10
References	S11

Table S1. Chemical composition of the metakaolin geopolymer.

Element	Concentration	Oxide	wt. %	Ref ¹
Si	17.70 mg/L	SiO ₂	58.1	54.5
Al	13.72 mg/L	Al ₂ O ₃	39.8	40.2
Ti	0.65 mg/L	TiO ₂	1.7	1.4
Fe	0.19 mg/L	Fe ₂ O ₃	0.4	1.8

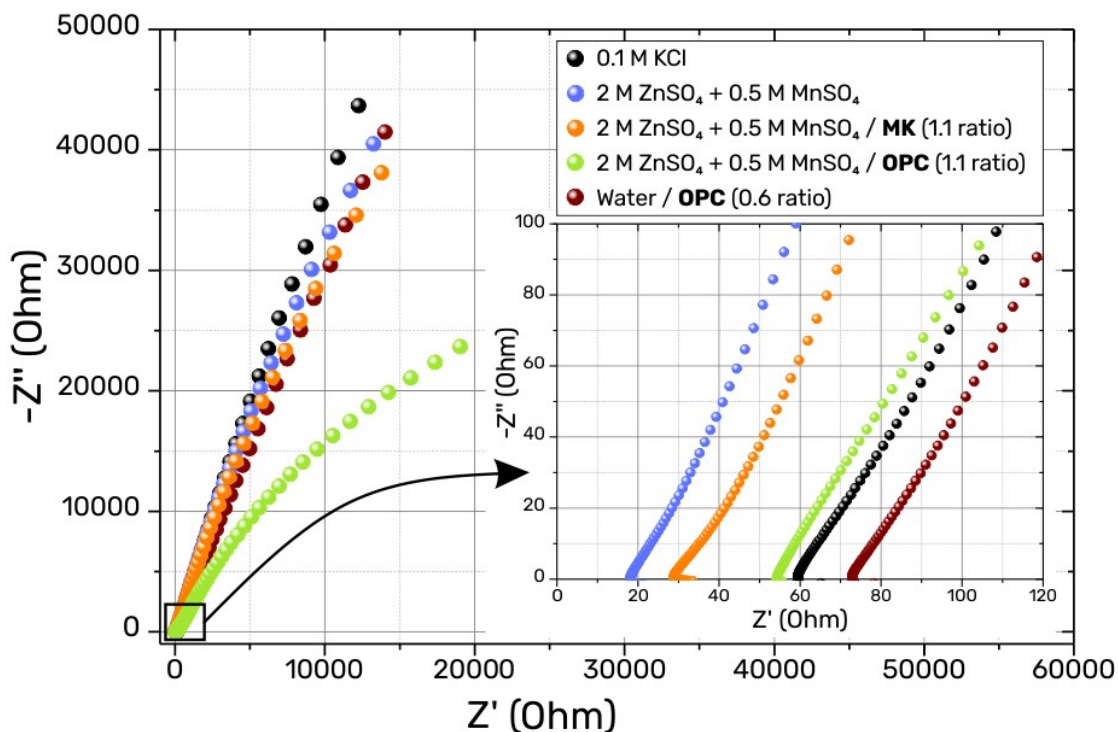


Figure S1. EIS spectra of various electrolytes at room temperature.

Table S2. Ionic conductivity of various electrolytes

Sample	Ionic conductivity ($\text{S}\cdot\text{cm}^{-1}$)
0.1 M KCl	1.223×10^{-2}
Aqueous 2M ZnSO ₄ + 0.5 M MnSO ₄	4.328×10^{-2}
2M ZnSO ₄ + 0.5 M MnSO ₄ / MK (1.1 ratio)	2.457×10^{-2}
2M ZnSO ₄ + 0.5 M MnSO ₄ / OPC (1.1 ratio)	1.339×10^{-2}
Water / OPC (0.6 ratio)	1.049×10^{-2}

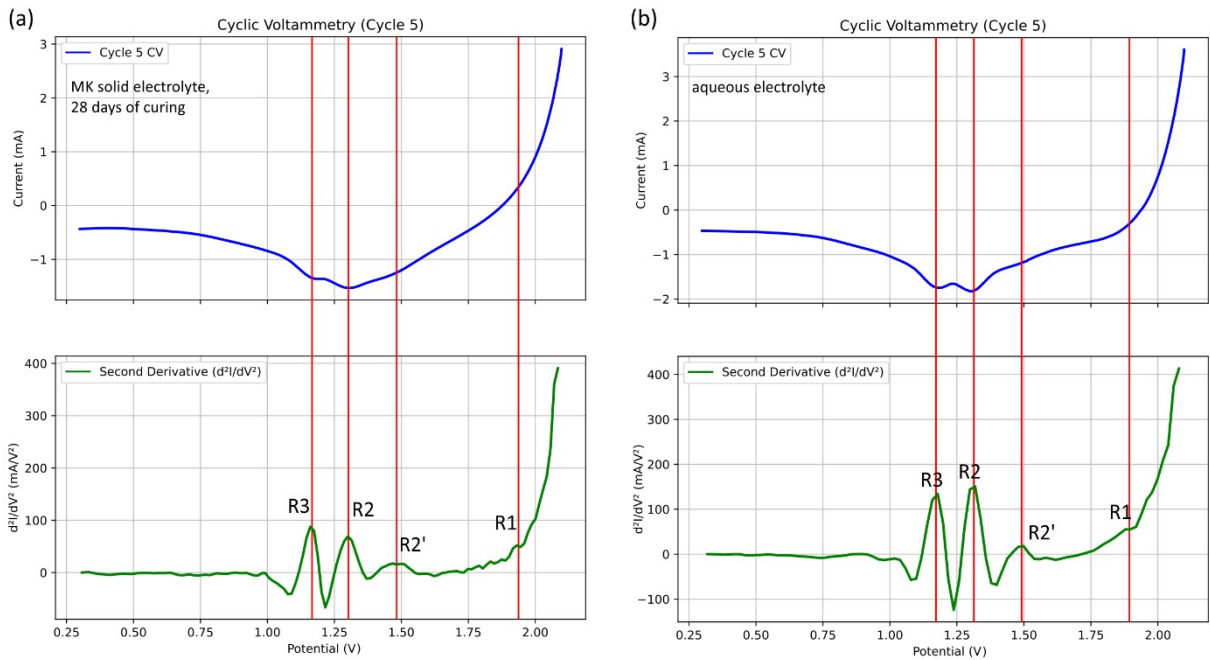


Figure S2. CV plots at 0.2 mV/s for cycle 5 (top) and the corresponding second derivatives for the battery with the MK electrolyte with 28-days curing time (a) and the battery with the aqueous electrolyte (b), allowing to identify all critical points in the measured CV curves.

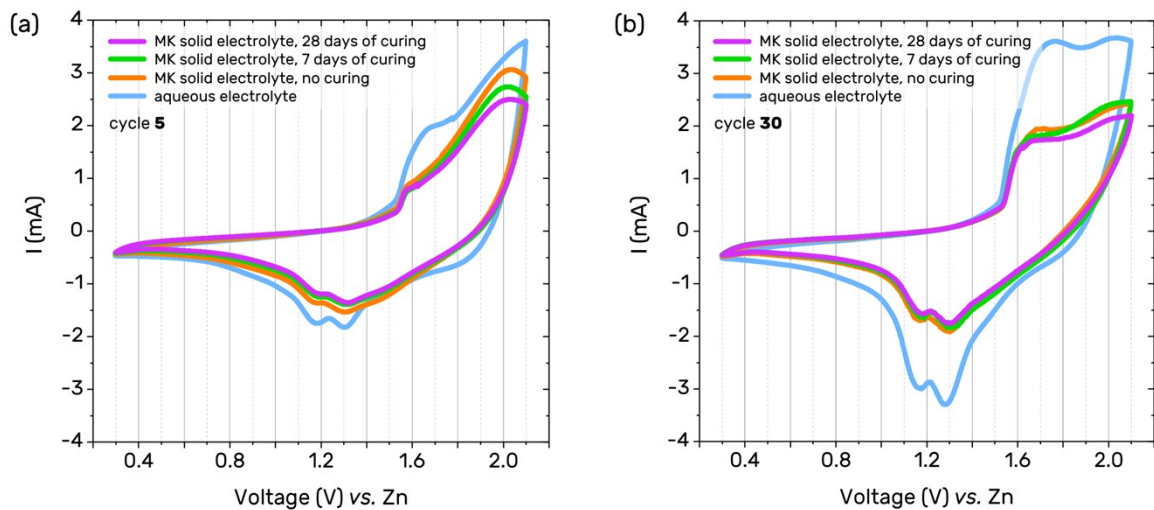


Figure S3. CV plots at 0.2 mV/s for cycle 5 (a) and cycle 30 (b) for four different cells: aqueous Zn/MnO₂ with a liquid 2M ZnSO₄ + 0.5 MnSO₄ electrolyte (blue), solid Zn/MK/MnO₂ with no curing time (orange), solid Zn/MK/MnO₂ after 7 days of curing (green), and solid Zn/MK/MnO₂ after four weeks of curing (magenta).

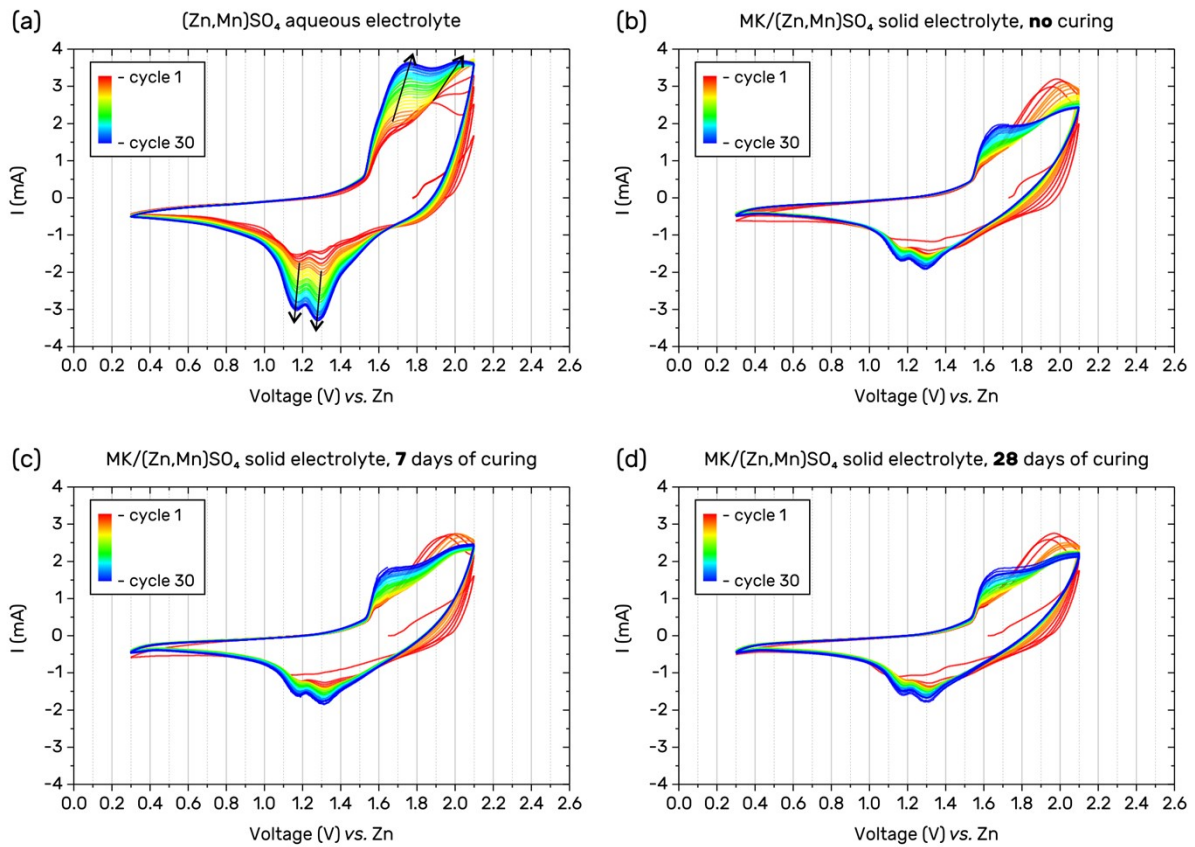


Figure S4. Evolution of the CV plots at 0.2 mV/s corresponding to four different cells: aqueous Zn/MnO_2 (a), solid $\text{Zn}/\text{MK}/\text{MnO}_2$ with no curing time (b), solid $\text{Zn}/\text{MK}/\text{MnO}_2$ after 7 days of curing (c), and solid $\text{Zn}/\text{MK}/\text{MnO}_2$ after four weeks of curing (d).

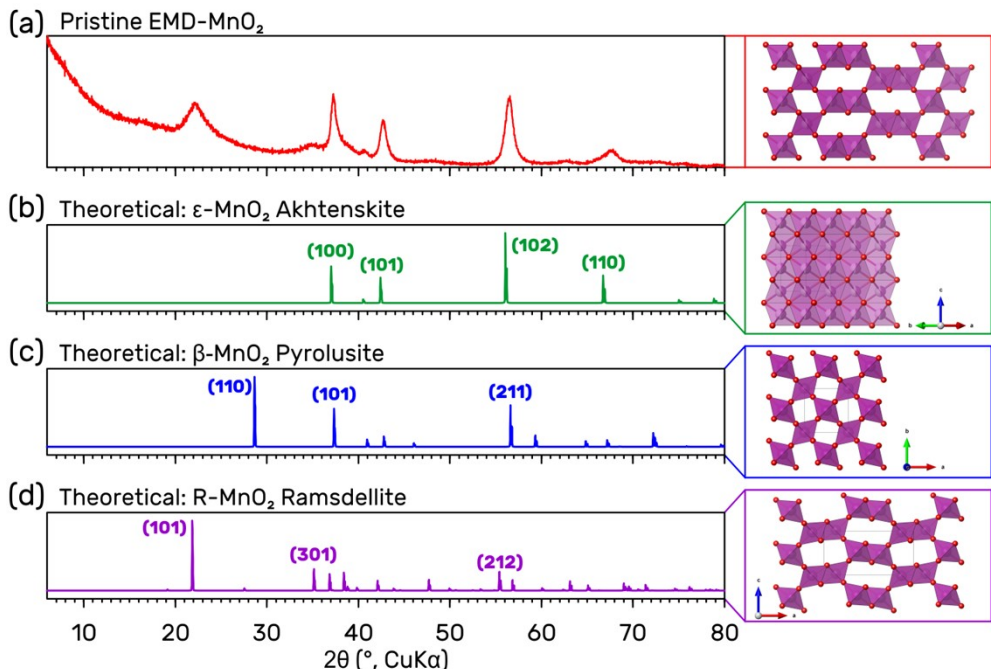


Figure S5. Experimental powder XRD pattern for EMD- MnO_2 and simulated XRD patterns for selected MnO_2 polymorphs: ϵ - MnO_2 ² (b), β - MnO_2 ³ (c), and R- MnO_2 ⁴ (d).

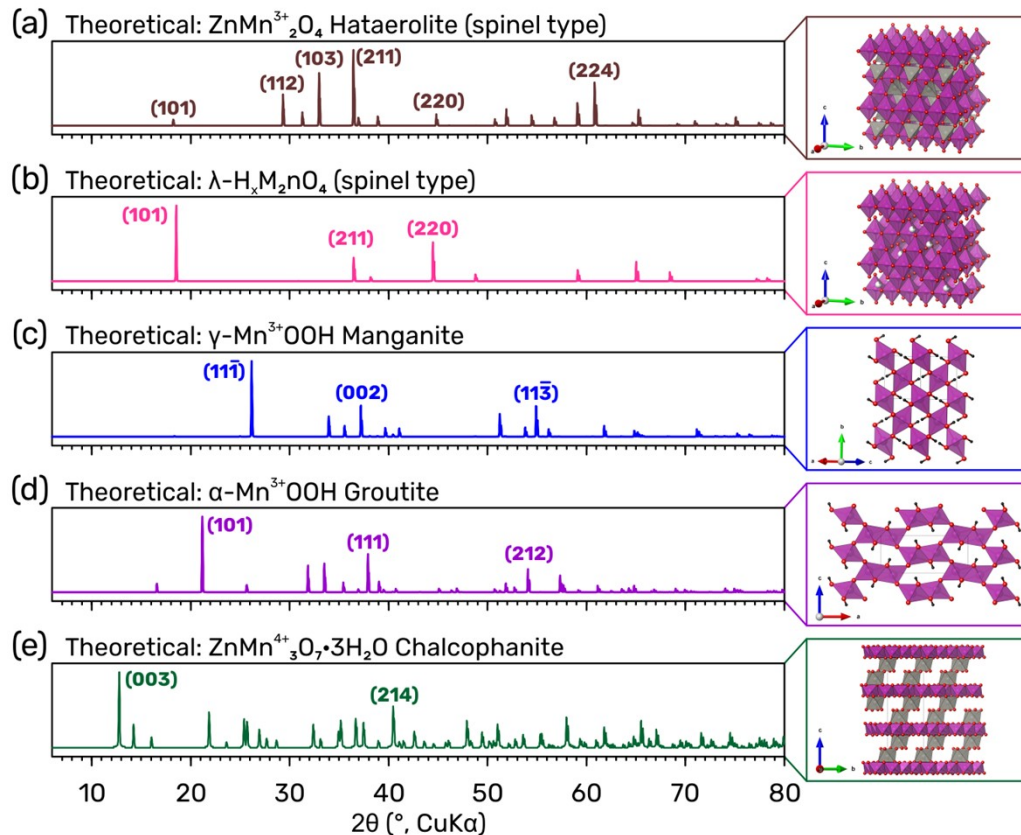


Figure S6. Simulated XRD patterns for selected Mn-containing phases reported in the Zn/MnO₂ system: ZnMn₂O₄⁵ (a), H_xMn₂O₄⁶ (b), γ -MnOOH⁷ (c), α -MnOOH⁷ (d), and ZnMn₃O₇(H₂O)₃⁸ (e).

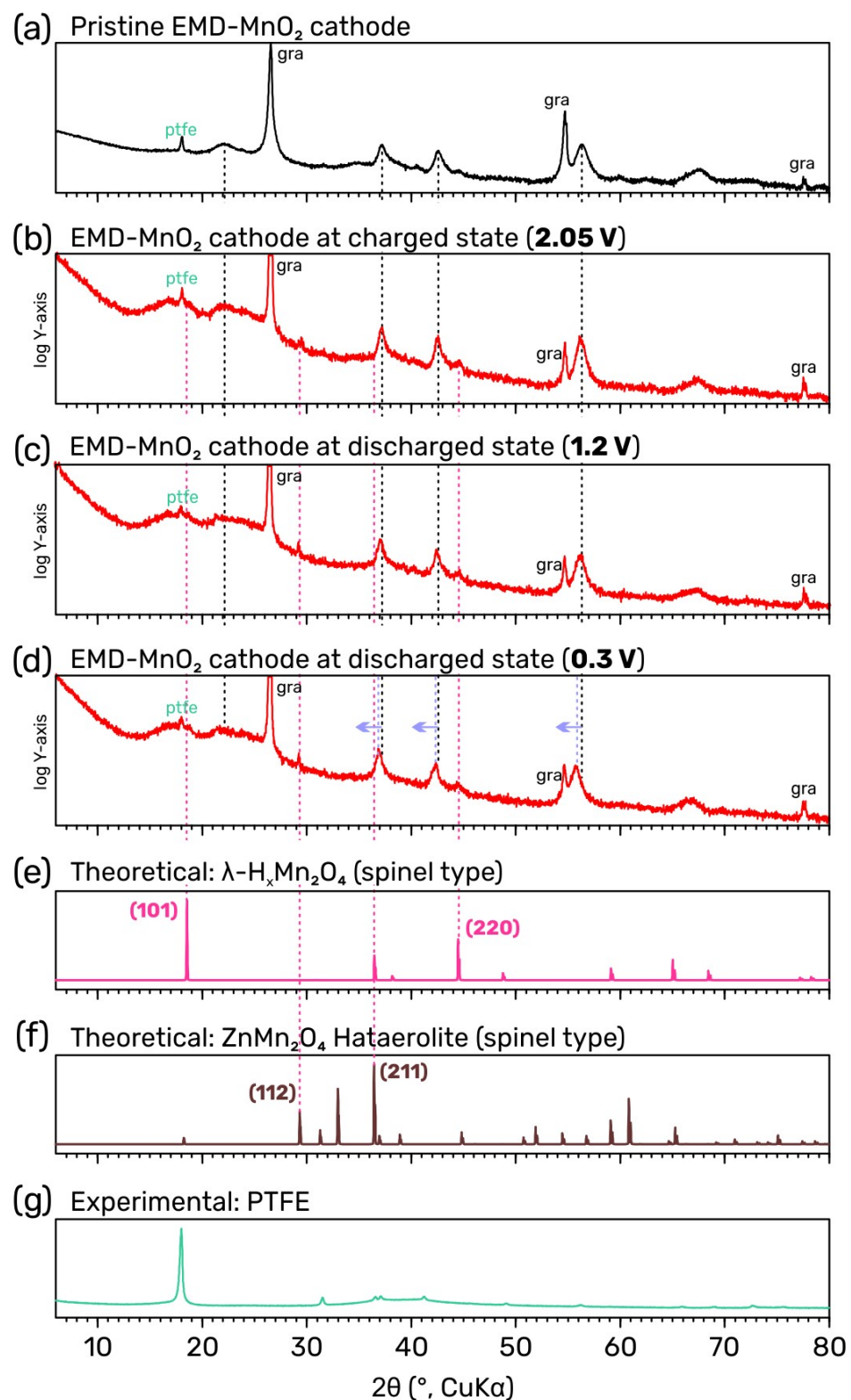


Figure S7. Phase identification in experimental *ex situ* XRD patterns of the MnO_2 electrode at different voltages upon electrochemical cycling, and comparison with the theoretical simulated patterns for $\text{H}_x\text{Mn}_2\text{O}_4$ ⁶ (b) and ZnMn_2O_4 ⁵ (f).

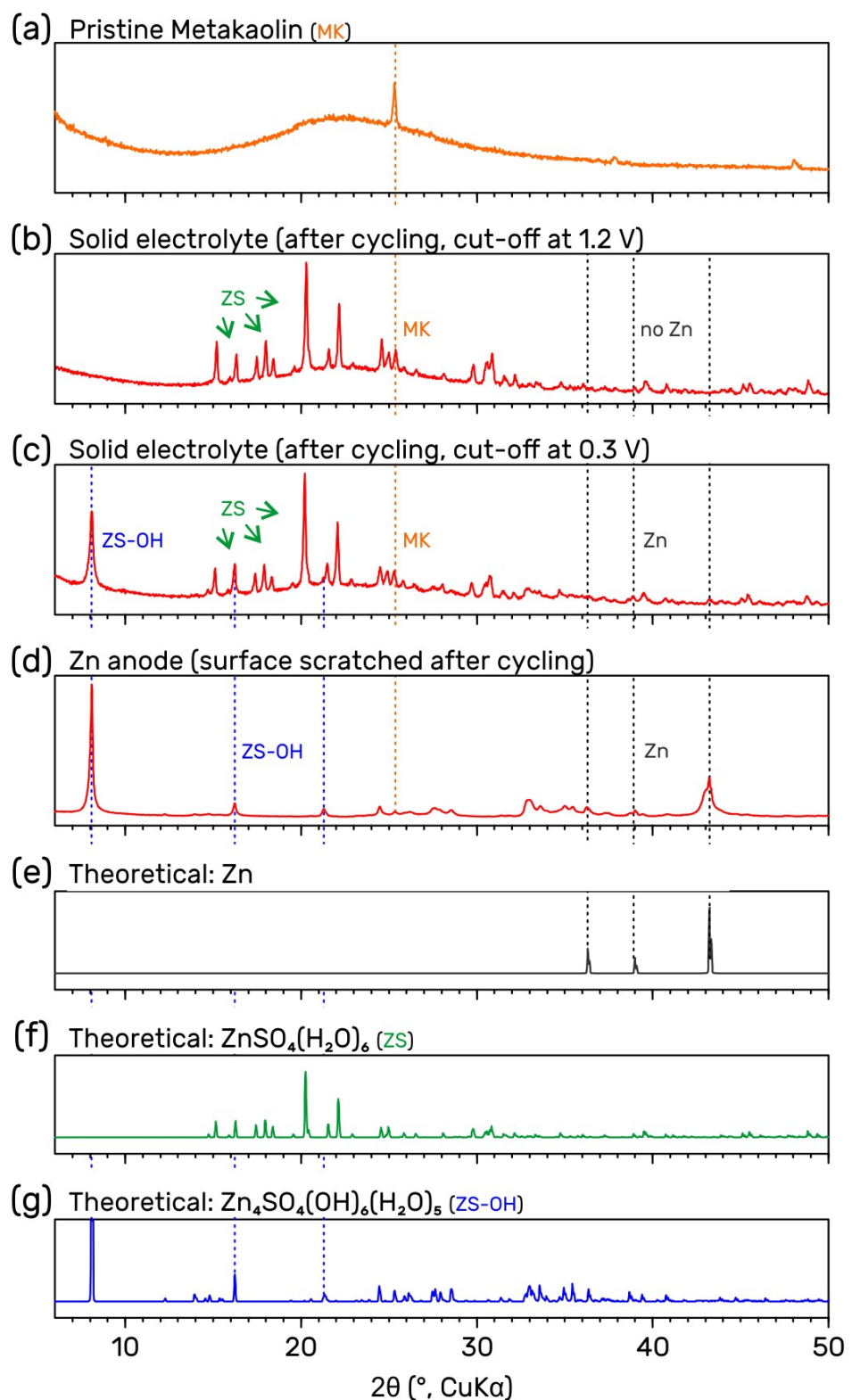


Figure S8. Phase identification in experimental *ex situ* XRD patterns of the solid electrolyte at different voltages upon electrochemical cycling, and comparison with the theoretical simulated patterns for Zn⁹ (e), $\text{ZnSO}_4(\text{H}_2\text{O})_6$ ¹⁰ (f), and $\text{Zn}_4\text{SO}_4(\text{OH})_6(\text{H}_2\text{O})_5$ ¹¹ (g).

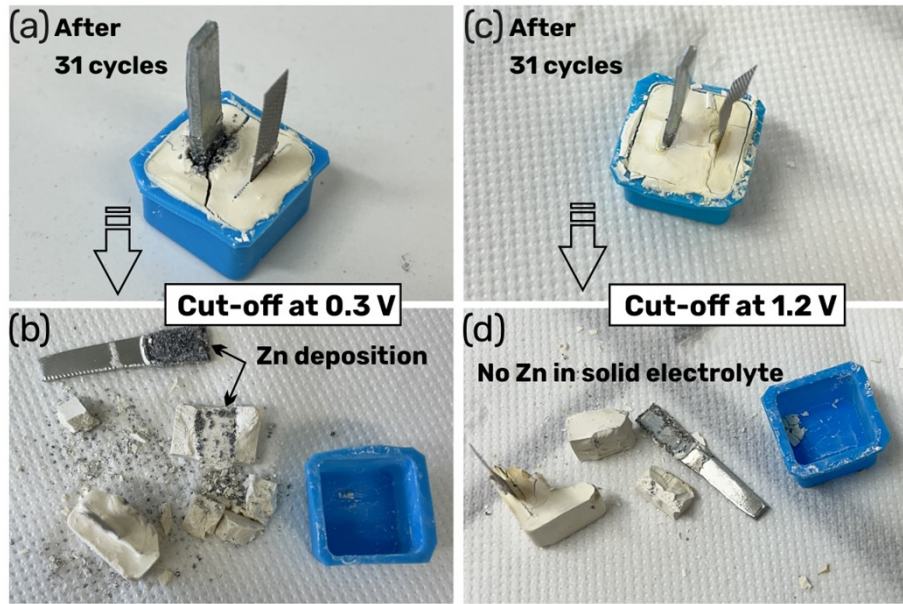


Figure S9. (a, c) Photos of the cell after 31 charge/discharge cycles. (b) Observation of Zn deposits on the negative electrode and in the metakaolin solid matrix with a cut-off voltage set at 0.3 V vs Zn. (d) Almost no Zn observed with a cut-off voltage set at 1.2 V vs Zn.

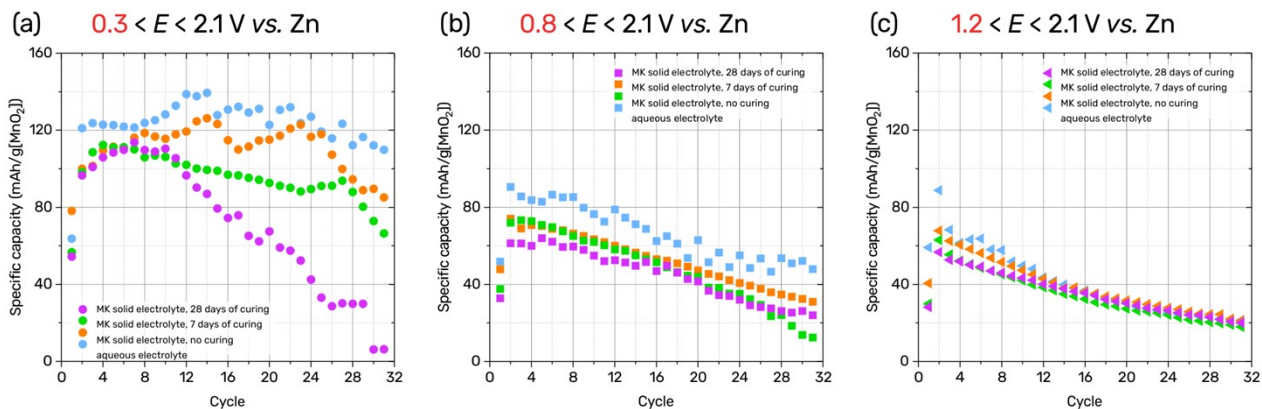


Figure S10. Specific capacity (in mAh/g of loaded MnO_2) versus cycle number in three voltage ranges at C/25: 2.1–0.3 V (a), 2.1–0.8 V (b), and 2.1–1.2 V vs Zn (c).

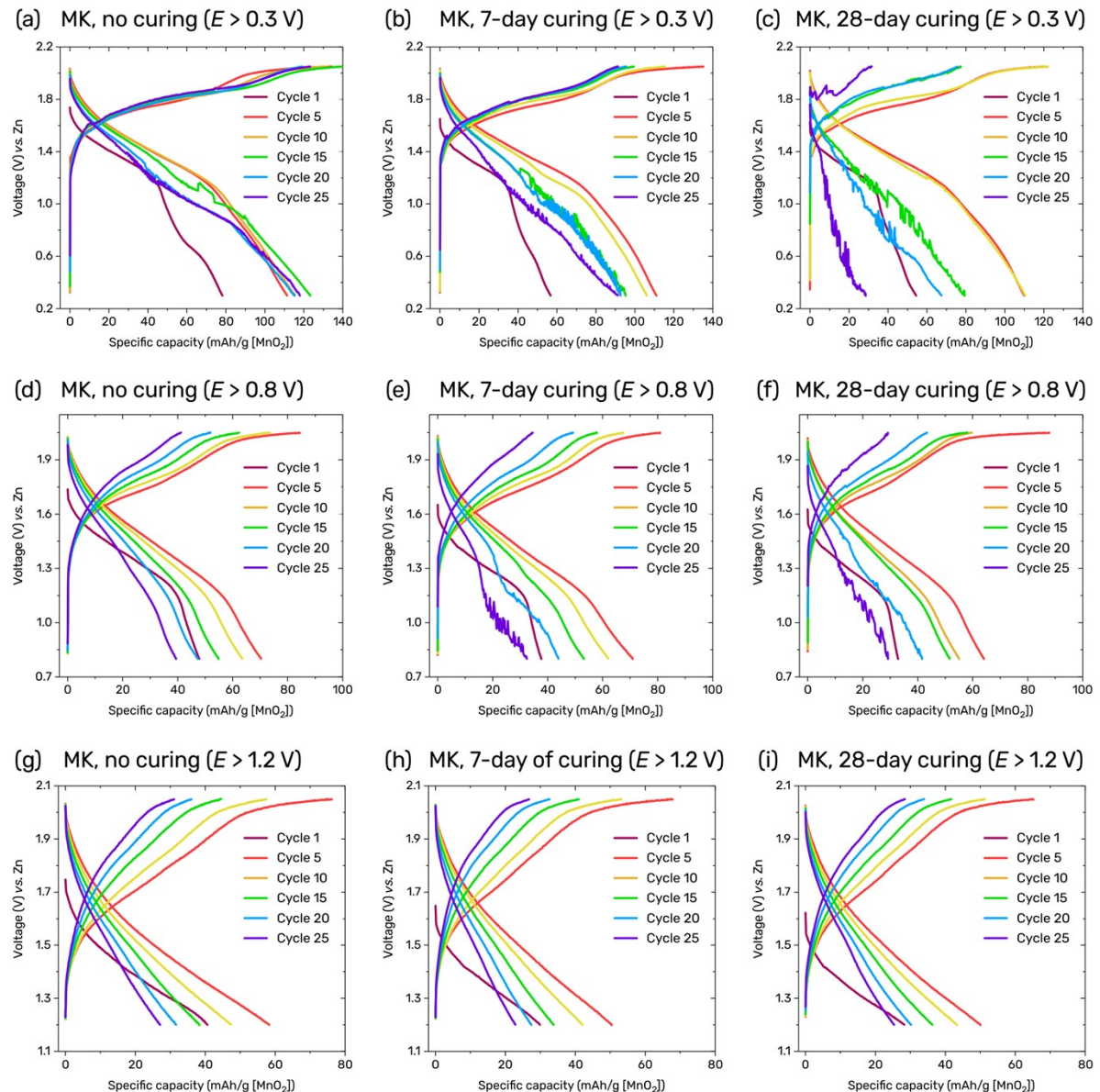


Figure S11. Charge/discharge curves at C/25 of the Zn/metakaolin/MnO₂ cells with different curing time and under various cycling conditions.

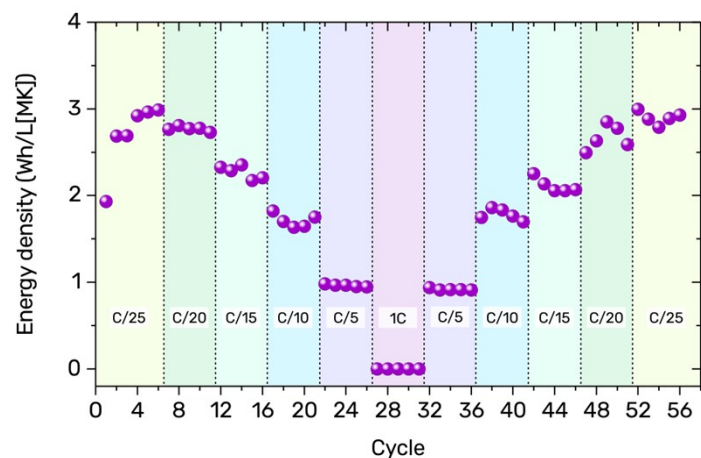


Figure S12. Current rate capabilities at C-rates from 0.04 to 1C for the cell with 28-days of curing time.

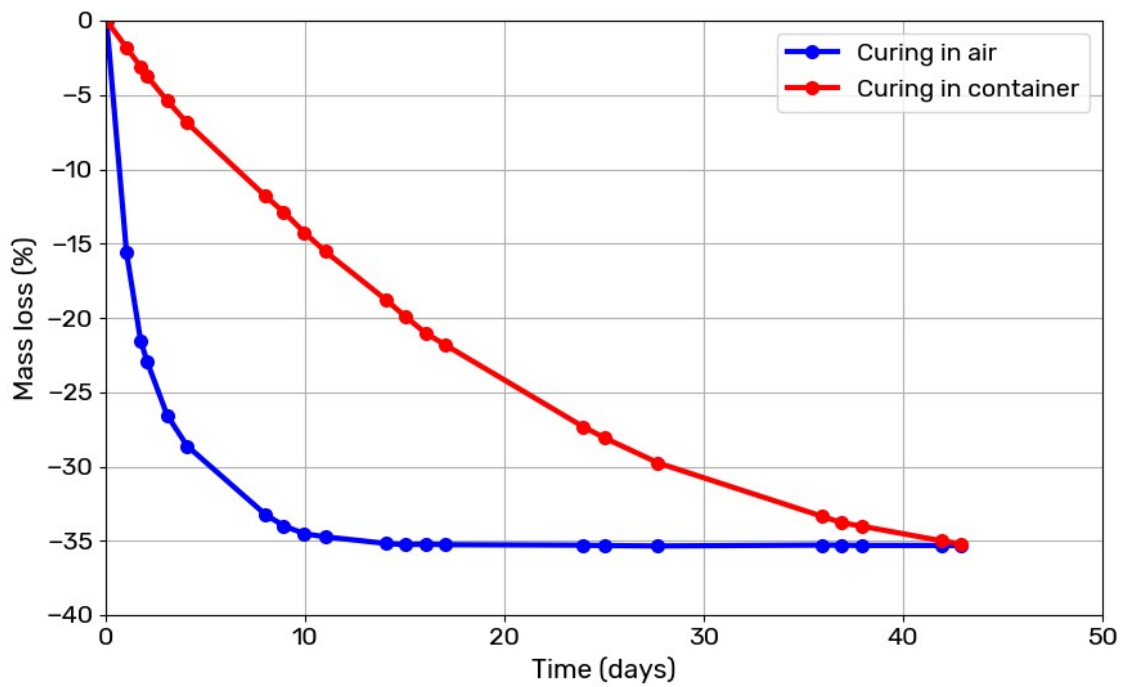


Figure S13. Mass loss of the metakaolin-based batteries over time.

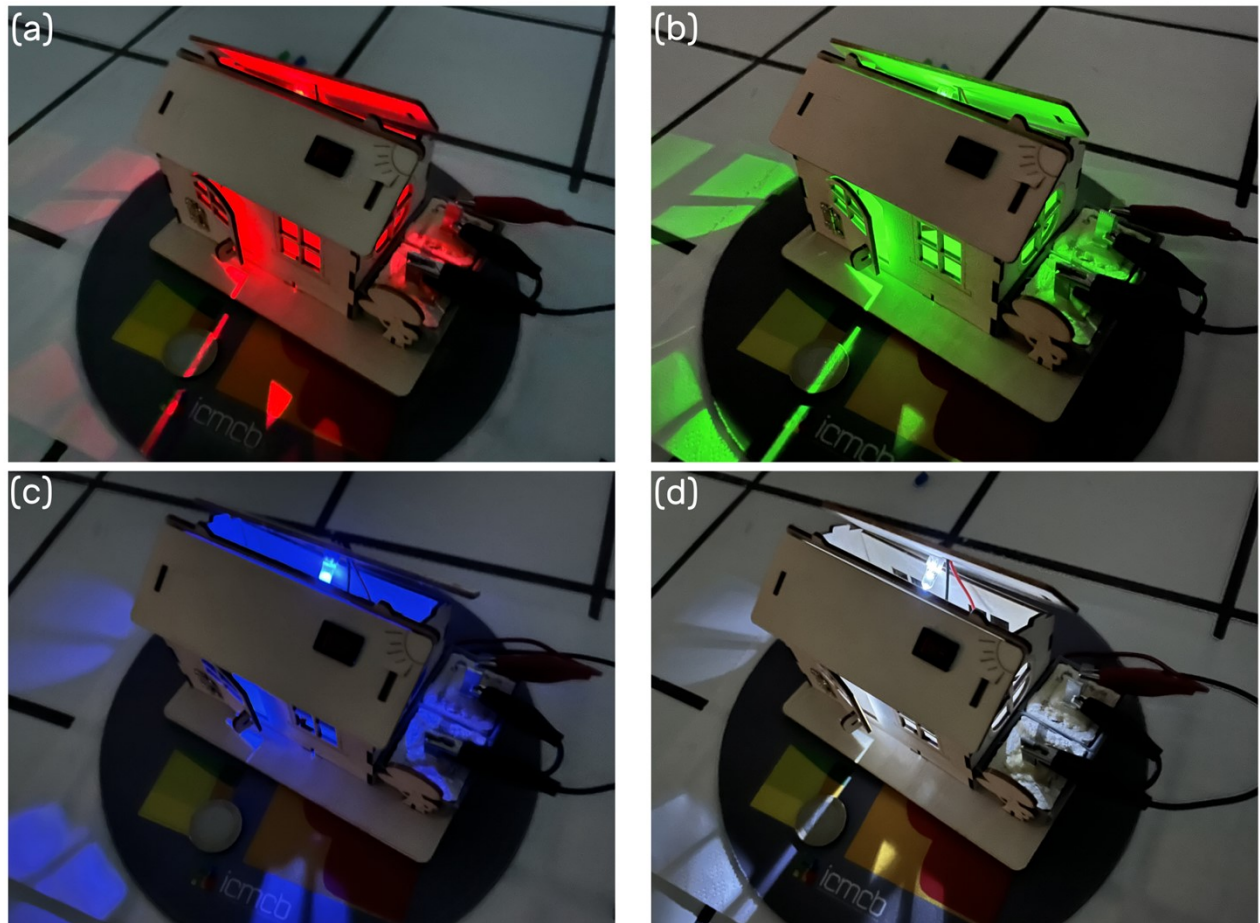


Figure S14. Powering red (a), green (b), blue (c), white (d) light-emitting diodes by two geopolymer cells connected in series.

References

- (1) Scherb, S.; Köberl, M.; Beuntner, N.; Thienel, K.-C. J. Neubauer, *Materials (Basel)*. **2020**, *13*, 2214.
- (2) Jiang, Y.; Yuan, L.; Wang, X.; Zhang, W.; Liu, J.; Wu, X.; Huang, K.; Li, Y.; Liu, Z.; Feng, S. *Angew. Chemie Int. Ed.* **2020**, *59*, 22659–22666.
- (3) Curetti, N.; Bernasconi, D.; Benna, P.; Fiore, G.; Pavese, A. *Phys. Chem. Miner.* **2021**, *48*, 43.
- (4) Post, J. E.; Heaney, P. J. *Am. Mineral.* **2004**, *89*, 969–975.
- (5) Patra, P.; Naik, I.; Bhatt, H.; Kaushik, S. D. *Phys. B Condens. Matter* **2019**, *572*, 199–202.
- (6) Ammundsen, B.; Jones, D. J.; Rozière, J.; Berg, H.; Tellgren, R.; Thomas, J. O. *Chem. Mater.* **1998**, *10*, 1680–1687.
- (7) Kohler, T.; Armbruster, T.; Libowitzky, E. *J. Solid State Chem.* **1997**, *133*, 486–500.
- (8) Post, J. E.; Appleman, D. E. *Am. Mineral.* **1988**, *73*, 1401–1404.
- (9) Masadeh, A. S.; Shatnawi, M. T. M.; Adawi, G.; Ren, Y. *Mod. Phys. Lett. B* **2019**, *33*, 1950410.
- (10) Spiess, M.; Gruehn, R. *Zeitschrift für Anorg. und Allg. Chemie* **1979**, *456*, 222–240.
- (11) Bear, I. J.; Grey, I. E.; Madsen, I. C.; Newnham, I. E.; Rogers, L. J. *Acta Crystallogr. Sect. B Struct. Sci.* **1986**, *42*, 32–39.